Available online at www.sciencedirect.com
SCIENCE DIRECT®
Pattern Recognition 38 (2005) 1295–1305
PATTERN RECOGNITION
THE JOURNAL OF THE PATTERN RECOGNITION SOCIETY
www.elsevier.com/locate/patcog

A system for human identification from X-ray dental radiographs☆

Omaima Nomir, Mohamed Abdel-Mottaleb*

Department of Electrical and Computer Engineering, University of Miami, 1251 Memorial Dr., Coral Gables, FL 33146, USA

Received 3 May 2004; received in revised form 16 December 2004; accepted 16 December 2004

Abstract

Forensic odontology is the branch of forensics that deals with human identification based on dental features. In this paper, we present a system for automating that process by identifying people from dental X-ray images. Given a dental image of a postmortem (PM), the proposed system retrieves the best matches from an antemortem (AM) database. The system automatically segments dental X-ray images into individual teeth and extracts the contour of each tooth. Features are extracted from each tooth and are used for retrieval. We developed a new method for teeth separation based on integral projection. We also developed a new method for representing and matching teeth contours using signature vectors obtained at salient points on the contours of the teeth. During retrieval, the AM radiographs that have signatures closer to the PM are found and presented to the user. Matching scores are generated based on the distance between the signature vectors of AM and PM teeth. Experimental results on a small database of dental radiographs are encouraging.

Keywords: Dental radiograph; Forensic odontology; Human identification; Image segmentation

1. Introduction

Under severe circumstances, such as those encountered in mass disasters (e.g., airplane crashes) or if identification is being attempted more than a couple of weeks postmortem, most physiological biometrics may not work, because of the decay of soft tissues of the body. Therefore, a postmortem biometric identifier has to resist the early decay that affects body tissues. Because of their survivability, the best candidates for postmortem biometric identification are the dental features. Forensic odontology [1] is the branch of forensics concerned with identifying humans based on their dental features obtained from dental radiographs. Dental features are very important as the best candidates for postmortem biometric identification [2]. Currently, the identification is carried out manually by comparing extracted features from a postmortem (PM) dental record to extracted fractures from a database of antemortem (AM) records. The forensic experts confirm the identity based on distinctive features such as dental restoration, dental work features, root morphology and teeth morphology [3,4]. In many cases these features are not enough to correctly identify individuals and this manual identification approach is useful only for verifying individuals in a small database.

The goal of our research is to automate the process of extracting a representation from the dental radiographs and to automate the process of matching PM and AM records [5–8]. This will facilitate for forensic odontologists to search through large numbers of AM records and only manually verify the few best matches.

☆ This research is supported in part by the US National Science Foundation under Award number EIA-0131079, the research is also supported under Award number 2001-RC-CX-K013 from the Office of Justice Programs, National Institute of Justice, US Department of Justice.

* Corresponding author. Tel.: +1 305 284 3825; fax: +1 305 284 4044.
E-mail addresses: onomir@umsis.miami.edu (O. Nomir), mottaleb@miami.edu (M. Abdel-Mottaleb).

0031-3203/$30.00
doi:10.1016/j.patcog.2004.12.010

In order to achieve this goal, we need to automate the process of segmenting the dental radiographs and to separate each individual tooth. The segmentation of dental images is difficult due to the shape variations and intensity variations within the same X-ray image and from one image to another. There is not much published work for dental image segmentation. In Refs. [9,10], segmentation of 3D images of dental plaster models was presented. In Ref. [11], segmentation based on active contours for low-contrast radiographs was described, where they start with an initial approximation using deterministic algorithms to improve the performance of the algorithm. The watershed algorithm was used in Ref. [12] to find orthodontic feature points such as cusps, apexes, and ridges of teeth from 3D profile of dental images of imprints. In Refs. [13,14], they proposed a method for X-ray image segmentation, pixel classification, and contour matching. They used a semi-automatic contour extraction method. For matching, they use Euclidean distance between the contours of the PM and AM images.

In this paper we present a new fully automated system for archiving AM dental images in a database, and for searching the database for the best matches to a given PM image. The AM images are archived by segmenting and separating the individual teeth in bite-wing images and then extracting a set of signatures for each tooth. The goal of the segmentation is to separate the teeth from the rest of the radiograph. Then the individual teeth are separated by first separating the upper jaw from the lower jaw and then separating each tooth, this step is achieved using integral projection [15,16]. After separating each tooth, salient points on the contour of each tooth are identified and signatures for these points are extracted using a new method. These signatures are vectors that are extracted for each salient point. During searching, matching scores are generated based on the distance between the signature vectors of AM and PM teeth. Experimental results show that our system performs well in separating each individual tooth form its surroundings. It also shows, on a small database of X-ray dental images, the performance of the system for human identification using dental radiographs.

Dental X-ray images are classified according to the view they are captured from and their coverage. The most commonly used images are panoramic, periapical, and bite-wing. Panoramic is taken to view complete upper and lower jaws, it does not show as fine details as do bite-wing and periapical. Periapical is captured to obtain a view of the entire tooth area including the tip of the root and the surrounding tissues. Bite-wing is captured to view back teeth, only the crowns and parts of the roots for two to four adjacent teeth in both upper and lower jaws are captured. The bite-wing images hold more information about the curvature, and the roots, and these images are the most common views made by dentists, therefore, we used them in our system.

The paper is organized as follows: In Section 2 we present the segmentation method, and the method for separating each individual tooth, in Section 3 we describe the shape matching method, in Section 4 the experimental results are presented, and Section 5 concludes the paper.

2. Radiograph segmentation and teeth separation

The first stage of the segmentation separates the teeth from the background using a two-step thresholding technique; this stage is detailed in Section 2.1. The second stage separates the upper jaw from the lower jaw and then separates each tooth using integral projection; this stage is detailed in Section 2.2. Fig. 1 shows a block diagram of the main steps of the segmentation algorithm.

2.1. Radiograph segmentation

In dental X-ray images there are variations from image to image due to variations in exposure. There are also variations from region to another within the same image, which makes the segmentation very challenging.

Dental X-ray images have three different regions: the background, which has the lowest intensity, corresponds to soft tissues. The bone areas have average intensity and the teeth have highest intensity. In some cases the intensity of the bone areas is close to the intensity of the teeth, which makes it difficult to use a single threshold for the whole image.

In Ref. [14], a probabilistic model is used to describe the gray level distribution for the teeth and the background pixels. For radiograph segmentation, a user-assisted initialization is needed to detect the gap valley between the upper and lower jaws. For tooth isolation, the gaps between the teeth were located by summing the intensity of the gray-scale pixels in each line perpendicular to the gap valley between the two jaws.

Our segmentation starts by iterative thresholding followed by adaptive thresholding [17,18] to segment the teeth from both the background and the bone areas. In Section 2.1.1 we present the iterative thresholding step, in Section 2.1.2 we present the adaptive thresholding step.

2.1.1. Iterative thresholding

The iterative thresholding is a modification of the method used in Ref. [19]. In Ref. [19], iterative thresholding was used to automatically segment CT lung images in order to accommodate the small variations that are expected across a population of subjects. They assume that the image volume contains only two types of voxels, the body voxels and non-body voxels. They start the algorithm by selecting the initial threshold based on the properties of the two volumes, i.e., pure air and the chest wall/body. In our technique, the initial thresholding is estimated by first detecting the edges in the original image using Canny edge detection [20]. Then, it applies a morphological dilation [21] to the binary edge image to obtain pixels around the edge locations. The reason for applying this step is to select the pixels around areas of

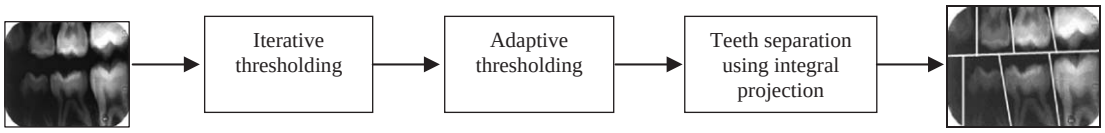

Fig. 1. The segmentation algorithm.

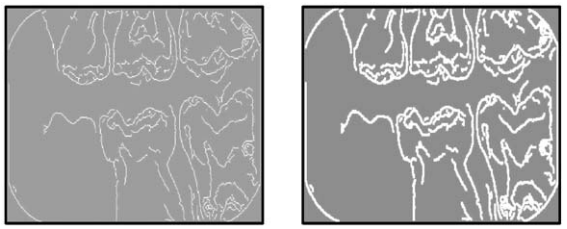

Fig. 2. (a) The binary edge image; (b) the dilated edge image.

high contrast in the original image. Usually, about half of the pixels in the resulting image will belong to the teeth areas and the other half will belong to the background and the bones. After obtaining the dilated image, we use the average gray value of the corresponding pixels from the original image, as an initial threshold. Fig. 2 shows the binary edge image for the image in Fig. 1 and the result of dilation. Then, the iterative thresholding is done as follows.

Let $f(i, j)$ be the gray-scale value at pixel (i, j), and T_i be the segmentation threshold at step i. To obtain a new threshold, we threshold the original image using T_i to separate the image into teeth areas and non-teeth areas, where μ_o^i and μ_B^i are the mean gray values for the two areas.

$$\mu_o^i = \frac{\sum_{(i,j)\in dental} f(i, j)}{\#dental\_pixels}, \tag{1}$$

$$\mu_B^i = \frac{\sum_{(i,j)\in background} f(i, j)}{\#background\_pixels}. \tag{2}$$

The threshold for step $i + 1$ is obtained as

$$T_{i+1} = \frac{\mu_B^i + \mu_o^i}{2}. \tag{3}$$

The iterative threshold updating step is repeated until there is no change in the threshold, i.e., $T_i = T_{i+1}$. The final threshold segments the image into teeth areas (pixels with values higher than the threshold) and background areas (pixels with values lower than the threshold). Four to ten iterations were found to be sufficient for convergence. Fig. 3 shows the resulting binary image for the image in Fig. 1. It also shows the result of masking the original image with the binary image, i.e., the ones in the binary image have been replaced with the original image gray values, and the zeros are kept. This is the image to which adaptive thresholding is applied.

A relative sensitivity analysis was done to study the effect of both the Canny hysteresis and the structuring element used by the morphological operations on the system performance. We randomly selected 50 images from the database to be our training set. For a large range of hysteresis values (0.01–0.5 for the minimum threshold, and 0.06–0.8 for the maximum threshold) with 100 samples for each value, we observed the relative change in the segmentation results. The results were found to be insensitive to the variations in Canny hysteresis values.

For the morphological operations, over a reasonable structuring element shapes, the best performance for the system was obtained when the structuring element is a 4-connected binary structuring element.

2.1.2. Adaptive thresholding

From the experimental results, applying the iterative thresholding technique to segment the teeth from the background sometimes did not lead to good results, e.g., see Figs. 12 and 13 in Section 4. Applying adaptive thresholding to the result of masking the original image (Fig. 3c) always produces more accurate results. We can notice that in Fig. 4 the teeth are separated better than in Fig. 3b, and that leads to correctly locate the separation lines between the teeth, as will be explained in Section 2.2.

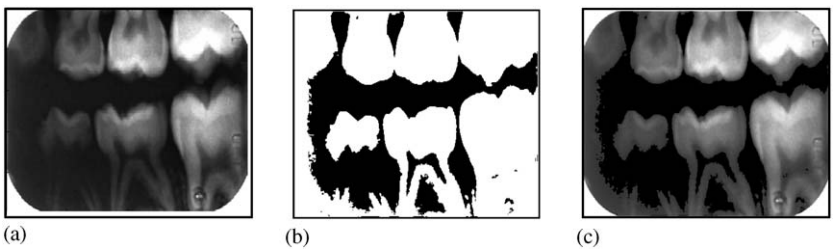

Fig. 3. (a) The original image; (b) result of iterative thresholding; (c) the original image after masking by the binary image.

The idea of the adaptive thresholding is to threshold the pixel at the center of a window according to the average gray value of the non-zero pixels inside this window. Using a window of size $I \times J$ pixels, the following is applied to each pixel of the image that results from masking the original image with the binary image obtained from the iterative thresholding.

$$T(i,j) = \frac{\sum_{s=-I/2}^{I/2} \sum_{t=-J/2}^{J/2} f(i+s, j+t)}{\#nonzero\_pixels}. \quad (4)$$

If the center pixel value of the window is $C(i,j)$, then

$$C'(i,j) = \begin{cases} 1, & C(i,j) \geqslant T'(i,j), \\ 0 & otherwise. \end{cases} \quad (5)$$

By randomly selecting 30 images from the database as our training set (these images were not used in testing), $T'(i,j) = 0.9 \times T(i,j)$ was found to be a suitable threshold value.

Fig. 4. Result of adaptive thresholding.

We compared the results of segmentation based on the above algorithm with the results obtained if we choose the initial threshold as average gray value of the whole image. The results of the above algorithm were consistently better. Figs. 5 and 6 show an example of the two results after applying the adaptive thresholding. In Fig. 5d some of the teeth parts are missing because the calculated average threshold value is biased to the gray value of the background. It is clear that the result in Fig. 6d is more accurate.

2.2. Teeth separation

After segmenting the teeth from the background, each tooth is separated from its surroundings in order to prepare for feature extraction. This is achieved by first separating the upper and the lower jaws, and then separating each tooth.

2.2.1. Separating the upper and the lower jaws

If we consider the image in Fig. 4, it is clear that a horizontal or a near horizontal line can separate the upper jaw and the lower jaw. This can be achieved by using horizontal projection as follows.

Let $f(i,j)$ be the $m \times n$ binary image obtained from the segmentation stage, the horizontal integral projection is

$$H(i) = \sum_{j=1}^{n} f(i,j). \quad (6)$$

Assuming that it is possible to separate the upper jaw from the lower jaw by a straight line, the integral projection

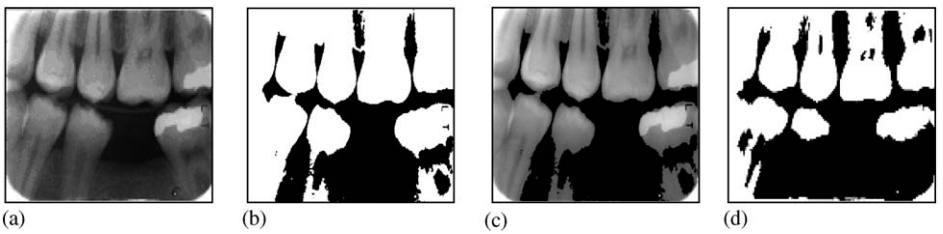

Fig. 5. (a) Original image; (b) the result from the original image after iterative thresholding; (c) the original image after masking by the binary image; (d) the result after adaptive thresholding.

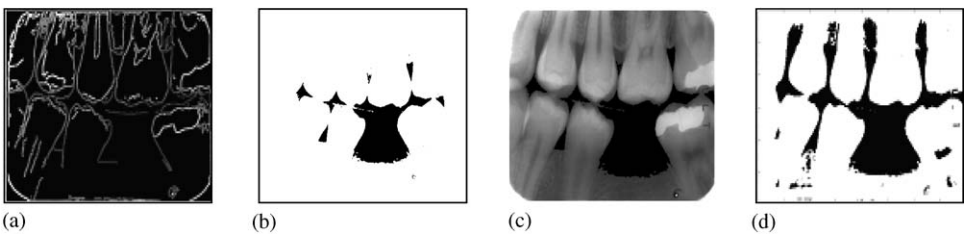

Fig. 6. (a) Gray-scale edge image; (b) the result for the gray-scale edge image after iterative thresholding; (c) the original image after masking by the binary image; (d) the result after adaptive thresholding.

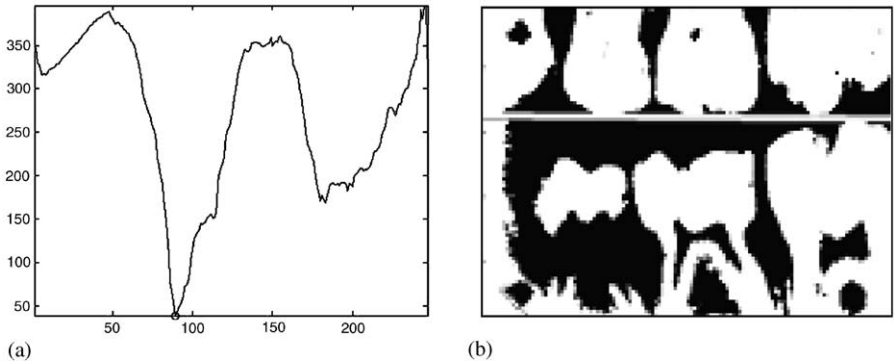

Fig. 7. (a) Horizontal integral projection; (b) the initial line segmenting the 2 jaws.

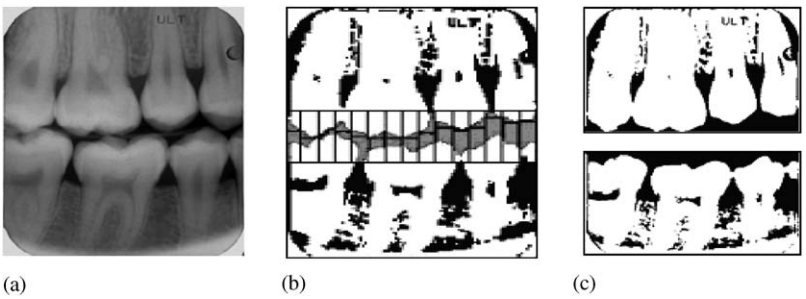

Fig. 8. (a) The original image; (b) the binary image with the exact locations for separating the two jaws; (c) the upper and the lower jaws after separation.

along that line will be minimal. Since it is not always the case that this line is horizontal, we need to rotate the image in a small range of angles, e.g. [−20: 20], and find an angle at which we obtain a line that produces the minimum horizontal projection. This is obtained as follows:

$$\theta, i = \arg \min_{\theta,i} H_\theta(i), \tag{7}$$

where $H_\theta(i)$ is the horizontal integral projection obtained by rotating $f(i, j)$ with an angle θ. Fig. 7 shows an example, in Fig. 7a the minimum horizontal projection point is marked with a circle, and Fig. 7b shows the corresponding horizontal line in the image. It is clear that this is the best horizontal line that can separate the two jaws without cutting through the teeth.

In many cases, there is no single straight line that can separate the upper and the lower jaws. Therefore, the initial straight line obtained from the horizontal projection is incrementally modified by reapplying the projection process in adjacent vertical strips in order to find the piecewise linear separation of the two jaws. The stripes are $h \times w$ pixels around the line, where h is the height of the strip and w is the width of the strip, in our experiments we used $h = 40$ and $w = 20$. Fig. 8 shows an example of separating the two jaws using this method. Fig. 8a shows a case where there is no single line that can separate the two jaws. Fig. 8b shows the result of using the piecewise separation method.

2.2.2. Separating each individual tooth

To separate each individual tooth we use a technique similar to the one used for separating the jaws. The goal is to find the lines that separate adjacent teeth. This can be achieved by using the integral projection method in the vertical direction. If $f(i, j)$ is the $m \times n$ binary image obtained from the segmentation stage, the vertical projection is

$$V(j) = \sum_{i=1}^{m} f(i, j). \tag{8}$$

The separating lines are located by finding valleys in the result of the vertical projection. Due to different teeth alignment, the lines are not always vertical nor parallel, see Fig. 4. Therefore, we rotate the image in a small range of angles, e.g. [−20: 20], and calculate the vertical projection for each angle in this range. For each projection, we use a threshold value to obtain the valleys that identify locations of vertical lines between adjacent teeth. In the experiments, we used a threshold value equal to 0.35 of the maximum number of ones in the result of the projection. We then select the

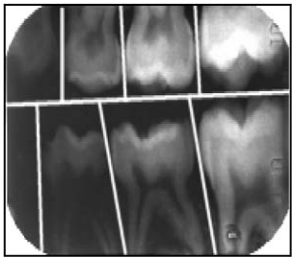

Fig. 9. Result of teeth separation.

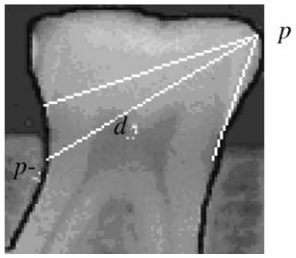

Fig. 10. Generating the signature vector V_p for point p.

separating lines and the corresponding angles which produce the minimum vertical projection among all the rotation angles.

Fig. 9 shows the detected separating lines overlaid over the original image.

3. Shape matching

We developed a new method for shape description and matching. It is similar to the algorithm that was introduced in Ref. [22] for surface matching. The method relies on selecting a set of salient points from the object's contour and generating a signature vector for each salient point. The signature vectors capture the curvature information for each salient point. Each element in the vector is the distance between the salient point and a point on the contour. Object matching is then performed by matching the signature vectors of the teeth. Salient points are identified as the points of high curvature on the contour.

In order to extract the contour pixels for each individual tooth, we first apply the technique used in Ref. [23] for the result of teeth separation to get ride of the remaining bone areas. Then, a connected component analysis using 8-connectivity [17] is applied to obtain the contour pixels. For all the teeth in the database as well as for the PM query teeth, each tooth contour is represented by equal number of points by applying equal points sampling technique on the extracted tooth contour pixels.

Fig. 10 shows an example, where the contour of the tooth is marked with black. The algorithm calculates the curvature for every point on the contour. Then selects the n points with the highest curvature as the salient points. A test is performed to eliminate spike points that have considerable higher curvature than its neighbors. These points are considered as noise. For each salient point, p, defined by its 2D coordinates, each other point p_i on the contour can be related to p by the distance

$$d_i = \|p - p_i\| \tag{9}$$

and the signature vector V_p of the point p is defined as

$$V_p = [\|p - p_i\|], \quad i = 1, \ldots, M, \tag{10}$$

where M is the number of points on the tooth contour.

This is done for all the N salient points, in the experiments we chose $N = 20$.

The matching is performed by calculating a matching distance between a PM image and an AM image based on the corresponding salient points.

Given a query PM tooth, and segmented AM tooth before matching it is important that the contours be represented w.r.t. the same coordinate system. This is achieved by removing variations which could be attributed to the allowed affine transformation [13,24], which is a function of the form

$$T(Q) = A \times Q + \tau, \tag{11}$$

where $Q = (x, y)^{\mathrm{T}}$ represents a point in the query contour, $T(Q)$ is the result of applying the affine transformation on Q. A is a transformation matrix that includes both rotation and scaling, and τ is a translation vector. The parameters A and τ can be represented as

$$A = \begin{pmatrix} \cos\theta & \sin\theta \\ -\sin\theta & \cos\theta \end{pmatrix} \times \begin{pmatrix} S_x & 0 \\ 0 & S_y \end{pmatrix}, \tag{12}$$

$$\tau = \begin{pmatrix} \tau_x \\ \tau_y \end{pmatrix}, \tag{13}$$

where θ is the rotation angle, S_x and S_y are vertical and horizontal scale factors, and τ_x and τ_y are vertical and horizontal translations. So, there is total of five parameters (i.e., $\theta, S_x, S_y, \tau_x, \tau_y$), they are optimized to obtain the best fit between the transformed query contour and the database contour. These parameters are obtained for two contours Q and Q', by minimizing

$$\begin{aligned} &\mathrm{E}(\theta, S_x, S_y, \tau_x, \tau_y) \\ &\quad = |T(Q) - Q'|^2 \\ &\quad = \sum_{i=1}^{M} (\cos\theta\, S_x x_i + \sin\theta\, S_y y_i + \tau_x - x_i')^2 \\ &\qquad + (\cos\theta\, S_y y_i - \sin\theta\, S_x x_i + \tau_y - y_i')^2, \end{aligned} \tag{14}$$

where M is the number of points on the contours.

By differentiating Eq. (14) w.r.t. each unknown parameter and set each result equal to zero, we have a system of equations which can be solved simultaneously for all considered parameters.

Now, suppose we have a query tooth contour, q, aligned with a database tooth contour, k, their signature vectors Q_i and K_i are defined as

$$Q_i = [\|qc_i - q_j\|], \quad i = 1, \ldots, N, j = 1, \ldots, M, \tag{15}$$

where qc_i is a high curvature point, q_j is a point on the contour, N is the number of high curvature points, and M is the number of points on the tooth contour,

$$K_i = [\|kc_i - k_j\|], i = 1, \ldots, N, j = 1, \ldots, M, \tag{16}$$

where kc_i is a high curvature point, and k_j is a point on the contour of the database tooth. The matching distance D to be minimized for each pair of query contour, q, and database contour, k, is

$$D = \sqrt{\sum_{i=1}^{N} \frac{1}{k'_i} \sum_{j=1}^{M} (Q_{i,j} - K_{i,j})^2}, \tag{17}$$

where $Q_{i,j}$ is element j in signature vector Q_i, $K_{i,j}$ is element j in signature vector K_i, and k'_i is the mean value for the database's signature vector i. k'_i is used to normalize the distance between each two corresponding signature vectors, i, for the distance D to be independent of the scale.

By ranking the values of D in an ascending order, the best matching AM tooth will correspond to the minimum D.

To increase the accuracy of our matching and reduce the search space when matching, we only consider corresponding teeth (i.e., teeth that have the same number). The teeth in all the images in the database are automatically classified and numbered according to the universal teeth numbering system (Fig. 11) using our algorithm in Ref. [25]. Given a PM query image, the teeth are first segmented, numbered and then matching is applied only to corresponding teeth in the database. This eliminates the possibility of matching teeth that have different numbers.

4. Experimental results

We have evaluated the performance of our system for teeth segmentation and separation; the results are presented in Section 4.1. Also we have evaluated the performance of the system for matching; the results are presented in Section 4.2.

4.1. Segmentation results

From the experimental results of the segmentation, using the adaptive thresholding after the iterative thresholding improves the final results in most of the images that have large intensity variation. Fig. 12 shows an example of using only iterative thresholding. In this example, some of the separating lines are missing. Fig. 13 shows improved result when the adaptive thresholding is used.

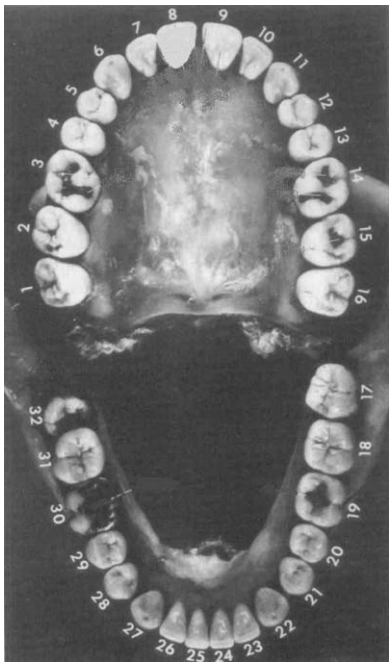

Fig. 11. Upper and lower jaws with teeth numbered according to the universal system.

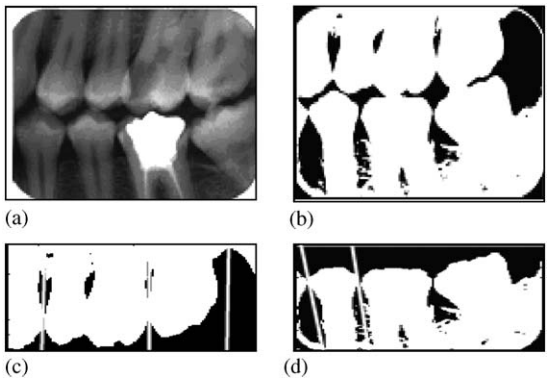

Fig. 12. (a) Original image; (b) result of iterative thresholding; (c) the upper jaw after locating the separating lines; (d) the lower jaw after locating the separating lines.

The proposed segmentation technique was applied to 117 bite-wing images. It always correctly segments the upper jaw from the lower jaw for all the images. Summary of the results for segmenting individual teeth are shown in Table 1. A few teeth segmentation/separation results are shown in Fig. 14.

The cases where teeth were not correctly separated are due to the poor quality of the images. This is especially true for teeth at the borders of the images. In these cases the method cannot correctly locate the separation lines, sometimes bones

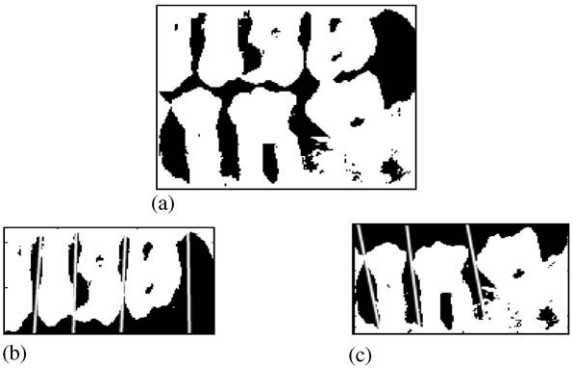

Fig. 13. (a) The image after adaptive thresholding; (b) the upper jaw after locating the separating lines; (c) the lower jaw after locating the separating lines.

Table 1
The segmentation results

	Upper jaw	Lower jaw
Total number of teeth in the 117 images	391	361
Number of correctly separated teeth	329	293
Ratio of correctly separated teeth	84%	81%

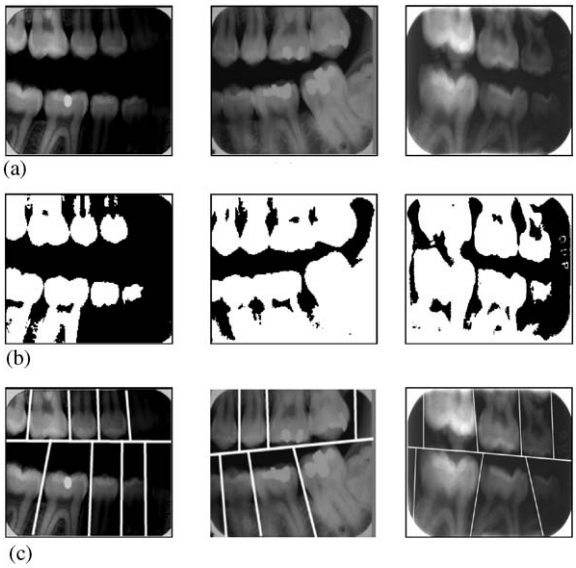

Fig. 15. Some cases where the segmentation technique fails; (a) the original images; (b) the images after applying adaptive thresholding; (c) the detected separating lines overlaid over the original image.

were considered as part of the tooth because of failure of the segmentation stage. Fig. 15 shows some cases.

4.2. Matching results

We tested our matching algorithm on a set of bite-wing dental images. The AM images were segmented, each tooth was classified, and the signatures of the individual teeth extracted and archived in a database. During matching, the query PM image is segmented, each tooth is classified, and the matching distance is calculated between a PM tooth and each AM tooth in the database with the same number. The best matched AM tooth is the one with minimum matching distance. Some X-ray AM images in the database are shown in Fig. 16.

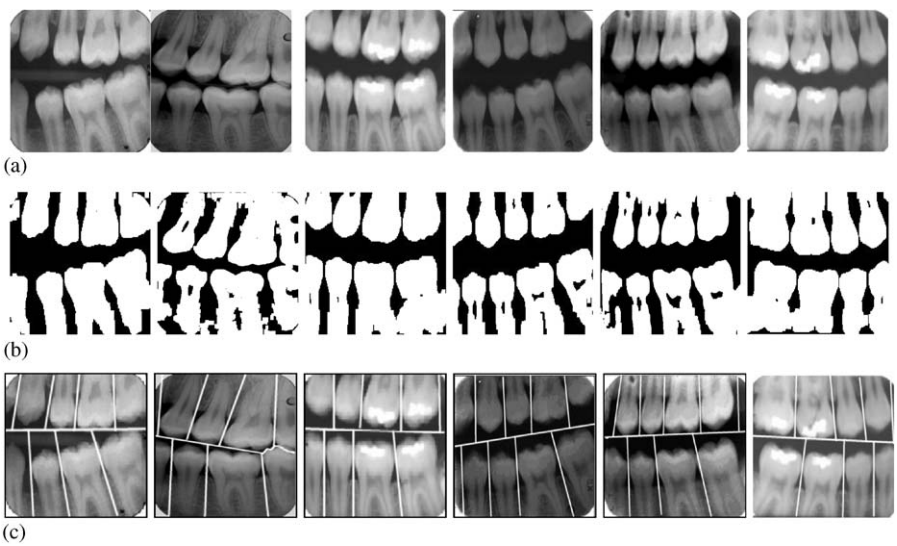

Fig. 14. Teeth segmentation and separation results; (a) the original images; (b) the images after applying adaptive thresholding; (c) the detected separating lines overlaid over the original image.

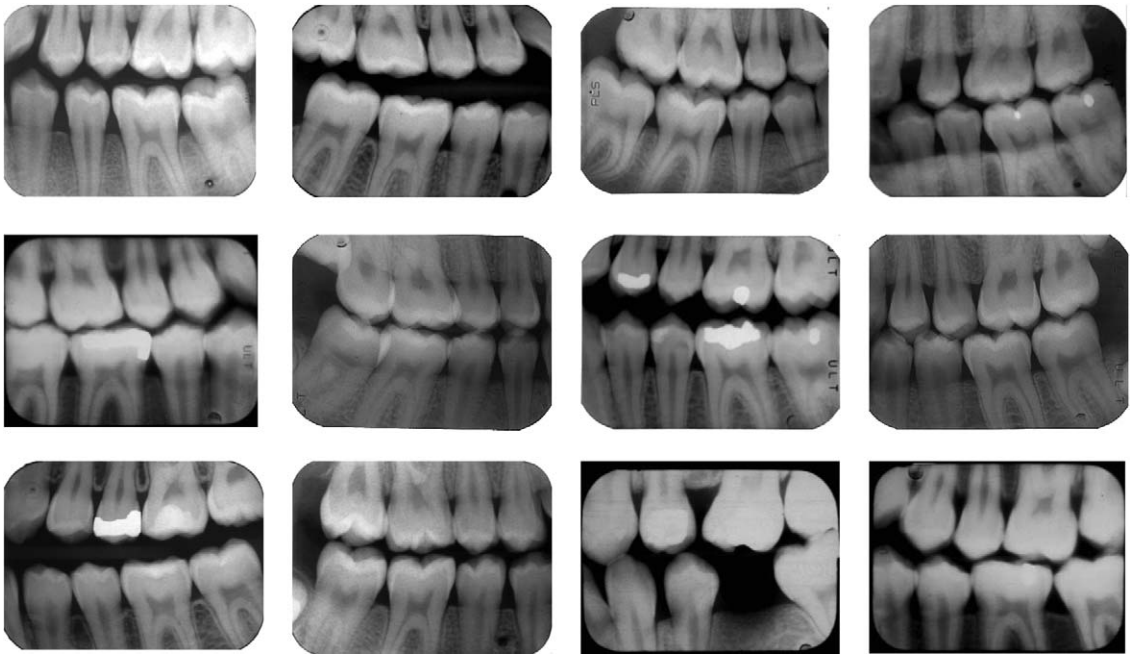

Fig. 16. Sample of X-ray AM images from the database.

The matching method was evaluated using 43 PM query images, which contain 139 teeth. The AM database contains 117 AM images. Among the 139 queries, 112 correct matches were ranked first based on the majority vote. The correct matches were always retrieved for the 43 PM query images, 35 were ranked first, three were ranked second, two were ranked third, and three were ranked fifth.

We apply the same matching technique to our testing set, but without applying the teeth classification step. Among the 139 queries, 106 correct matches were ranked first. The correct matches were also retrieved for the 43 PM query images, 32 were ranked first, three were ranked second, three were ranked fourth, two were ranked sixth, and three were ranked seventh. We can notice that applying the classification step improves the results beside decreasing the search space.

Fig. 17 shows the retrieval results for one of the query PM images, the left column shows the query tooth, the middle contains the retrieved tooth without using the classification and numbering technique and the right column contains the retrieved tooth when using the classification technique before matching. The matching distance D is listed under each retrieved tooth. The PM image in Fig. 17a contains six teeth, Fig. 17b shows four out of six teeth are correctly matched to an AM image of the same person. Fig. 17c shows five out of six teeth are correctly matched.

In order to obtain the best matching image, majority voting is used so that the best matching AM image is the image with the maximum number of teeth ranked first. In our example five out of six teeth were retrieved from the same image, therefore, it is considered the best match.

The mismatched results were mainly due to the poor quality of the images, which results in inaccurate contours. Another reason that can affect the results is that the PM images might be captured long time after the AM images were captured. In this case the shape of the teeth can change because of artificial prosthesis, teeth growth, and teeth extraction.

5. Conclusion and future work

In this paper we presented a system for automatic human identification based on dental radiographs. The system includes a new method for teeth separation and a new method for teeth shape description and matching. In our system, we use the bite-wing images because they are the most common views made by dentists. The system archives the AM images into a database by segmenting the teeth, extracting their contours, numbering the teeth using our algorithm introduced in Ref. [25], and representing each tooth by a set of signature vectors. Given a PM image, matching scores are calculated based on the distances between the signature vectors of AM and PM teeth. We have shown experimental results for the segmentation and the matching techniques. The system performance was tested on different quality images. Poor quality of the images was the main reason for the cases where the correct matches were not ranked first. If the system presents to the user the top 10 ranked images, the precision for the results that we obtained is 100%.

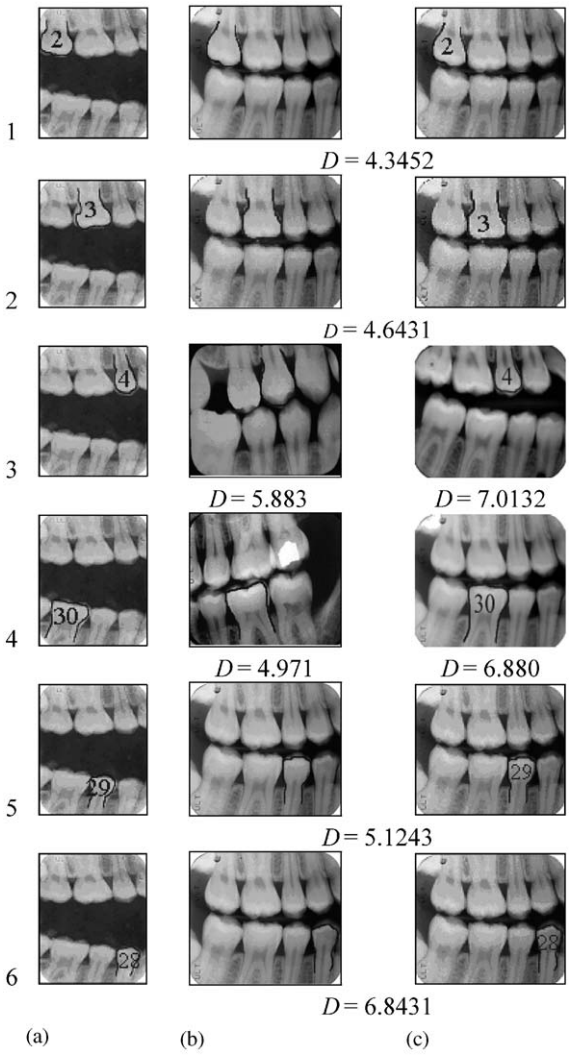

Fig. 17. Retrieval results; (a) query tooth marked with black; (b) best matching tooth in the database (1, 2, 5, and 6 are correct matches); (c) best matching tooth in the database when using classification and numbering technique (1, 2, 4, 5, and 6 are correct matches).

We analyzed the time complexity of the segmentation and matching algorithms. The time complexity of the segmentation algorithm is in O(lmn), where $l \times l$ is the window size used in the adaptive thresholding, and $m \times n$ is the image size. The time complexity of the teeth matching method is O(MN), where M is the number of points on a tooth contour, and N is the number of high curvature points.

Currently, we are also working on including panoramic and periapical radiographs in our database.

References

[1] American Society of Forensic Odontology, Forensic Odontology News, vol. 16, No. 2, Summer 1997.

[2] L. Hong, A. Jain, S. Pankanti, Biometric identification, Commun. ACM 43 (2) (2000) 91–98.

[3] United States Army Institute of Dental Research, Walter Reed Army Medical Center, Computer assisted post mortem identification via dental and other characteristics, USAIDR Information Bulletin, vol. 5, No. 1, Autumn 1990.

[4] B.G. Brogdon, Forensic Radiology, CRC Press, Boca Raton, 1998.

[5] M. Flickner, B. Scassellati, S. Alexopoulos, Retrieving images by 2D shape: a comparison of computation methods with human perceptual judgments, SPIE J. 2185 (1994) 2–14.

[6] L.F. Costa, R.M. Cesar, Shape Analysis and Classification: Theory and Practice, CRC Press, Boca Raton, FL, 2000.

[7] C.L. Huang, D.H. Huang, A content based image retrieval system, Image Vision Comput. 16 (1988) 149–163.

[8] T. Zhang, W. Lu, J. Peng, Adaptive image matching via varying gray-level correction, IEEE Trans. Commun. 43 (5) (1995) 1970–1981.

[9] D. Paulus, M. Wolf, S. Meller, H. Niemann, Three dimensional computer vision for tooth restoration, Med. Image Anal. 3 (1) (1999) 1–19.

[10] T. Kondo, S.H. Ong, J.H. Chuah, Robust arch detection and tooth segmentation in 3D images of dental plaster models, Proceeding of IEEE Workshop on Medical Imaging and Augmented Reality, June 2001, pp. 241–246.

[11] M. Piotrowski, P.S. Szczepaniak, Active contour based segmentation of low-contrast medical images, International Conference on Advances in Medical Signal and Information Processing, 2000, pp. 104–109.

[12] M. Mokhtari, D. Laurendeau, Feature detection on 3D images of dental imprints, Proceedings of IEEE Workshop on Biomedical Image Analysis, June 1994, pp. 287–296.

[13] A.K. Jain, H. Chen, S. Minut, Dental Biometrics: Human Identification Using Dental Radiographs, AVBPA, UK, 2003, pp. 429–437.

[14] A.K. Jain, H. Chen, Matching of dental X-ray images for human identification, Pattern Recognition July(2004) 1519–1532.

[15] R. Brunelli, T. Poggio, Face Detection Through Geometrical Features, Massachusetts Institute of Technology, Cambridge, MA, USA, 1992.

[16] R. Brunelli, T. Poggio, Face recognition: features versus templates, IEEE Trans. Pattern Analysis Mach. Intell. (1) (1993) 1042–1052.

[17] R. Gonzalez, R. Wood, Digital Image Processing, Addison Wesley, Reading, MA, 1993.

[18] E. Davies, Machine Vision, Academic Press, New York, 1990 pp. 91–96.

[19] S. Hu, E.A. Huffman, M. Reinhardt, Automatic lung segmentation for accurate quantization of volumetric X-Ray CT images, IEEE Trans. Med. Imaging 20 (6) (2001) 490–498.

[20] R. Jain, R. Kasturi, B.G. Schnck, Machine Vision, McGraw-Hill Inc., New York, 1995.

[21] C. Giardina, E. Doughetr, Morphological Methods in Image and Signal Processing, Prentice-Hall, Englewood Cliffs, NJ, 1988.

[22] S. Yamany, A. Farag, Adaptive object identification and recognition using neural networks and surface signatures, IEEE Conference on Advanced Video and Signal Based Surveillance, 2003.

[23] J.D. Zhou, M. Abedl-Mottaleb, Automatic human identification based on dental X-ray images, Proceedings of the SPIE Conference on Defense and Security, Biometric Technology for Human Identification, 2004.
[24] T. Cootes, C. Taylor, Statistical models of appearance for computer vision, Technical Report, Wolfson Image Analysis Unit, Imaging Science and Biomedical Engineering, University of Manchester, UK, 2000.
[25] M. Mahoor, M. Abdel-Mottaleb, Classification and numbering of teeth in bitewing dental images, Pattern Recognition 38 (2005) 577–586.

About the Author—MOHAMED ABDEL-MOTTALEB received his Ph.D. in Computer science from University of Maryland, College Park, in 1993. He is an Associate Professor in the Department of Electrical and Computer Engineering, University of Miami, where his research focuses on 3D face recognition, dental biometrics, visual tracking, and Human activity recognition. Prior to joining the University of Miami, from 1993 to 2000, he worked at Philips Research, Briarcliff Manor, NY. At Philips Research, he was a Principal Member of Research Staff and a Project Leader, where he led several projects in image processing, and content-based multimedia retrieval. He holds 20 US patents and published over 60 papers in the areas of image processing, computer vision, and content based retrieval. He is an Associate Editor for the Pattern Recognition journal.

About the Author—OMAIMA NOMIR received her B.S. and M.S. degrees in Computer Science from the Department of Computer Science and Automatic Control, Alexandria University, Egypt. She is currently a Ph.D. student in the Department of Electrical & Computer Engineering, University of Miami, FL, USA. Her research interests include Pattern Recognition, Medical Image Processing, and Neural Networks.